Anomalous swelling of lipid bilayer stacks is caused by softening of the bending modulus

Nanjun Chu,[1] Norbert Kučerka,[1] Yufeng Liu,[1] Stephanie Tristram-Nagle,[2] and John F. Nagle[1,2]

[1]*Department of Physics, Carnegie Mellon University, Pittsburgh, Pennsylvania 15213, USA*
[2]*Department of Biological Sciences, Carnegie Mellon University, Pittsburgh, Pennsylvania 15213, USA*

Arrays of bilayers of the lipid dimyristoylphosphatidylcholine (DMPC) exhibit anomalous swelling as the temperature decreases from $T=27$ °C toward the main phase transition at $T_M=24$ °C, within the fluid L_α thermodynamic phase. Analysis of diffuse x-ray scattering data from oriented stacks of biological lipid bilayers now makes it possible to obtain the bending modulus K_C and the bulk compressibility modulus B separately. We report results that show that the measured bending modulus K_C for DMPC decreases by almost a factor of 2 between $T=27$ °C and the transition temperature at $T_M=24$ °C, which is the same temperature range where the anomalous swelling occurs. We also report Monte Carlo simulations that show that the anomalous swelling can be fully accounted for by the measured decrease in K_C with no changes in the van der Waals or hydration forces.

I. INTRODUCTION

Multilamellar arrays of many lipid bilayers are important in biophysical studies because they scatter strongly, thereby providing data for structural studies. Such data consist of the intensities of traditional Bragg peaks for samples that occur in low temperature phases [1], or that are often deliberately partially dehydrated [2]. In contrast, for fully hydrated samples in the most biologically relevant, disordered L_α phase, the scattering intensity becomes diffuse [3], which has led to new methods of data analysis [4–10].

The stacking of bilayers necessarily implies interactions between neighboring bilayers. Membrane interactions are of biophysical interest for discussing membrane fusion and other associations of membranes and to understand the effective forces between mesoscale structures [11,12]. The phenomenon of anomalous swelling, which has received considerable attention in the literature [13–25], provides a stringent test of our understanding of these interactions. Figure 1 shows the well-established temperature dependence from many measurements [19–21,23–25] for the repeat spacing D in fully hydrated multilamellar vesicles of bilayers of dimyristoylphosphatidylcholine (DMPC) which has 14 carbons in each hydrocarbon chain. Anomalous swelling also occurs in other lipids that have phosphatidylcholine headgroups and different numbers of carbons [13,14,19,22,25].

Current views ascribe three kinds of interbilayer interactions to bilayers composed of electrically neutral lipids [11,26]. First is a van der Waals attraction between neighboring bilayers that stabilizes the stacking. Second is a repulsive short range "hydration" interaction that decays exponentially [11]. Third is an entropic or fluctuational free energy repulsion due to the increased entropy that flexible bilayers can obtain by increasing the spacing between them [27]. For fully hydrated L_α phase samples, the hydration force is weak, and it is the competition between the attractive van der Waals interaction and the repulsive fluctuational interaction that primarily determines the repeat spacing D.

It was first proposed that the anomalous swelling of D for DMPC was due to a decrease in the bending modulus K_C

[25]; this would increase undulations, hence would increase the repulsive fluctuational interaction. This sensible hypothesis was in agreement with earlier theory [28] that predicted a decrease in the modulus for area expansion K_A, which is thought to be proportional to K_C [29]. However, x-ray measurements on powder MLV samples (multilamellar vesicles fully immersed in liquid water) did not indicate any anomaly or increase in the Caillé fluctuational η parameter. They did indicate that the bilayer became thicker as temperature was lowered to T_M [24], as predicted by theory [28]. Indeed, deuterium NMR measurements showed that there is the expected thickening of the hydrocarbon part of the bilayer due to increased order in the hydrocarbon chains [21], also supported by a neutron scattering study of unilamellar vesicles [18], earlier NMR data [30], and x-ray data [31]. This thickening of the bilayer accounts for nearly half the increase in D
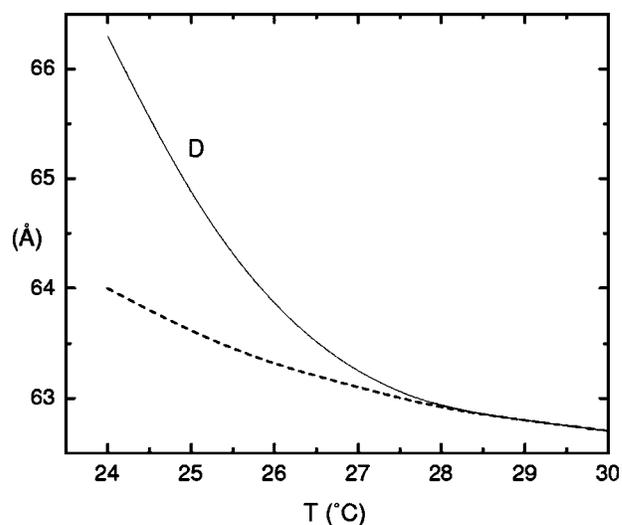
FIG. 1. Composite sketch from many papers for repeat spacing D versus temperature for DMPC is shown by solid line. The temperature dependence of the thickness of the bilayer is shown by the dashed line and is called the nonanomalous swelling. The difference is called the anomalous swelling [21].

041904-1

from 30 to 24 °C [21] as is indicated on Fig. 1, but it does not account for all the swelling. The remaining swelling between the solid and dashed lines in Fig. 1 that occurs between the transition temperature $T_M=24$ and 27 °C has been called the anomalous swelling [21]. A recent paper also used the term anomalous to describe the nonlinear part of the swelling of the bilayer thickness [14]; this usage emphasizes the important point that both the swelling of the bilayer and the additional swelling exhibit the same underlying critical phenomenon. For convenience in this paper, however, we will reserve the phrase anomalous swelling for the difference between the two lines in Fig. 1.

Direct testing of the hypothesis that a decrease in K_C causes the anomalous swelling has not been easy. A recent paper [15] used x-ray data that obtained the Caillé η parameter from MLV powder samples. Because

$$\eta = \pi k_B T/(2D^2 \sqrt{BK_C}) \tag{1}$$

involves both K_C and the compression modulus B, an ambitious extrapolation had to be performed using data at different osmotic pressures to estimate K_C and B separately [15]. The result for K_C shown in Fig. 9 of [15] was essentially constant except for one point right at T_M. Although it was concluded that anomalous swelling is caused by a decrease in K_C [15], such a decrease should have begun three degrees above T_M, near 27 °C where the anomalous swelling begins. Another recent study [32], while not addressing the anomalous swelling issue, reported K_C as a function of temperature for DMPC from oriented samples. (As was shown by Lyatskaya *et al.* [9], K_C and B can be separately obtained for biological lipids if oriented samples are used instead of MLV samples.) Although it was emphasized that there were inconsistencies in the experimental data, results were reported for K_C as a function of T in Fig. 4(c) of [32], which showed almost no change in K_C as a function of temperature for DMPC and none that has the same temperature dependence as the anomalous swelling. It may also be noted that the temperature dependence of the compression modulus B increased by a factor of 2 near T_M in [32] but decreased by 15% in [15]. An entirely different approach measured K_C on fluctuating giant unilamellar vesicles (GUVs) [33]. Lower values of K_C were obtained near T_M, but the values of K_C at 30 °C were considerably larger than other values obtained on GUVs [29] and values from multilamellar systems that we report here and that others have reported [15,32]. A more recent GUV study found a smaller K_C at one temperature near T_M, but this study focused on the broad sweep from the gel phase through to the L_α phase and did not resolve the temperature dependence within the anomalous swelling regime [34]. Swelling of the water space has also recently been reported for two supported bilayers and order of magnitude decreases in K_C have been deduced [16,17]. The fact that the swelling temperature T_S was several degrees below T_M was attributed to a lower transition temperature in the supported bilayers, but it was also acknowledged [16,17] that it could be due to rippling of the upper bilayer that forces a large water spacing, in which case the effect and the apparent values of K_C that were extracted are unrelated to anomalous swelling in the L_α phase. To resolve these many uncertainties

and inconsistencies, we have undertaken a study using oriented samples from which we obtain K_C as a function of T, directly and unambiguously, on multilamellar stacks. These stacks have equivalent interactions to MLV samples and both exhibit the same anomalous swelling.

II. EXPERIMENT

Oriented samples were prepared using the rock and roll method [35]; 10 mg of DMPC (Avanti Polar Lipids) in a chloroform:trifluoroethanol mixture $(1:1, v:v)$ was deposited onto a flat $15 \times 30 \times 1$ mm^3 Si substrate and subjected to shear during evaporation of the organic solvent. Such samples have been shown to be about 10 μm thick (consisting of nearly 2000 bilayers in the stack) and to have greater than 80% orientation [1]. The samples were trimmed to a strip that occupied only the central 5 mm of the 15 mm width of the substrate.

Each sample was mounted on a rotatable stage inside a specially designed sample chamber with the short 5 mm dimension along the x-ray beam direction, defined to be the y direction. The beam was set to 1.2 mm high (z direction) and 0.28 mm wide (x direction) using slits, so about 100 fresh spots were available on the sample by translation of the sample chamber along the x direction perpendicular to the beam. This capability was used to avoid radiation damage that begins to become apparent in our setup after about 10 min of x-ray exposure. The maximum rotation angle was 5°, so the entire 5 mm short length of the sample was contained in the footprint of the beam for all rotation angles.

A wavelength of 1.172 Å (10.58 keV) was set using the Osmic double bounce multilayer monochromator on the D1 station at CHESS (Cornell High Energy Synchrotron Source) with energy dispersion of 1.2% full width at half maximum (FWHM). Higher harmonics were reduced to less than 1% by detuning the double bounce monochromator with a resulting reduction in intensity of about 50%. Angular divergence was 1.4×10^{-4} rad in the horizontal direction and 1×10^{-4} rad in the vertical direction; these give transverse coherence lengths $L_x^C = 4300$ Å and $L_y^C = 6000$ Å [36]. The relevant coherence length along the normal to the stack of bilayers (which is not what is often called the longitudinal coherence length [36]) is given by $L_z^C = \pi\lambda/(q_z)\Delta\lambda$ [37]. For the largest q_z values used in our analysis L_z^C was limited by the energy dispersion to 600 Å.

Scattering intensities were collected on a MedOptics charge-coupled device (CCD) that has 1024×1024 pixels with average linear size 47.19 μm. The raw data were dezingered, dark CCD levels were subtracted, and the images were corrected for CCD geometric distortion and intensity distortion [38]. Exposure times were typically 60 s for each of the two images used for dezingering and two dezingered sets of data were obtained before moving to a different spot on the sample. Background images were obtained from a bare Si substrate. They were normalized to the data images using the beam intensity, which was recorded on all CCD images after attenuation by a 200 μm thick molybdenum semitransparent beam stop.

Most of our data were taken while the sample was rotated uniformly back and forth between $\theta = -5°$ and $+5°$ at con-
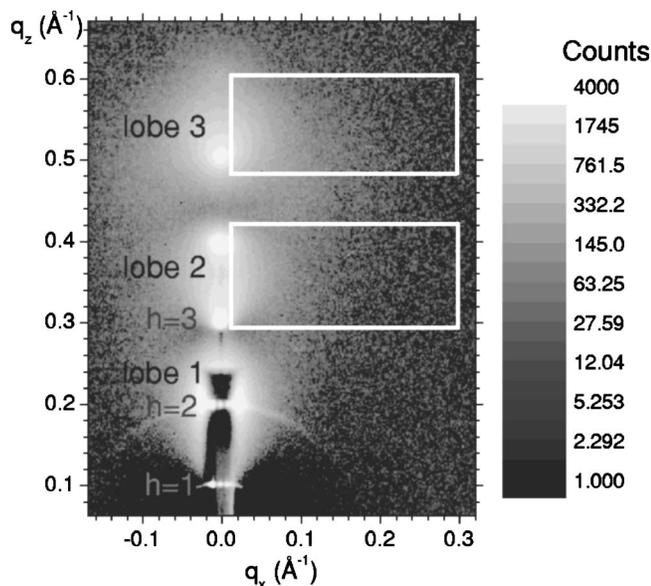
FIG. 2. Logarithmic gray scale CCD image of fully hydrated, uniformly rotating, oriented DMPC sample at 27 °C with background scattering subtracted. The strong first two orders are attenuated by a factor of about 2000 by an absorber to prevent overexposure of the CCD. The two white boxes show the regions of purely nonspecular scattering, uncontaminated by specular reflectivity, that is analyzed to obtain the material parameters K_C and B. This image was cropped from the original which extended from $q_z = -0.5$ to 0.95 Å^{-1} and $q_r = \pm 0.5$ Å^{-1}.

stant angular speed 20°/s in order to obtain scattering for all significant values of q_z on one CCD image. The exception was to measure mosaic spread by performing rocking scans that consisted of very short exposures at an increasing sequence of fixed sample angles θ centered around the angle θ_2 for the second order peak. Intensities were summed within a square region of 5×5 pixels, corresponding to the beam width in the x direction and the broadening due to the energy dispersion in the z direction, that was centered on the value of $2\theta_2$ for the $h=2$ peak. The rocking curve obtained as a function of the sample angle θ had a central width of 0.12° (FWHM) when fitted to a Gaussian; this gives the mosaic spread that was used in the analysis of the data.

The maximum intensities of the raw data in the regions used for analysis were typically four times greater than the background. Subtraction of the background images removed most of the background intensity in regions of the CCD where no scattering from the sample was anticipated. However, there was still a small, smooth increase in intensity with increasing q_z that was removed by a final background subtraction using interpolation of the data from regions with large enough q_x that the intensity did not vary with q_x, i.e., regions where diffuse scattering was negligible. Figure 2 shows one such background subtracted data set. We also note that the air in the sample chamber was replaced with helium to reduce background scattering from the beam.

Hydration of the sample was through water vapor in equilibrium with bulk water in the bottom of the sample chamber, so the beam did not have to travel through bulk water or any condensed matter except for four thin 6 μm Mylar windows.
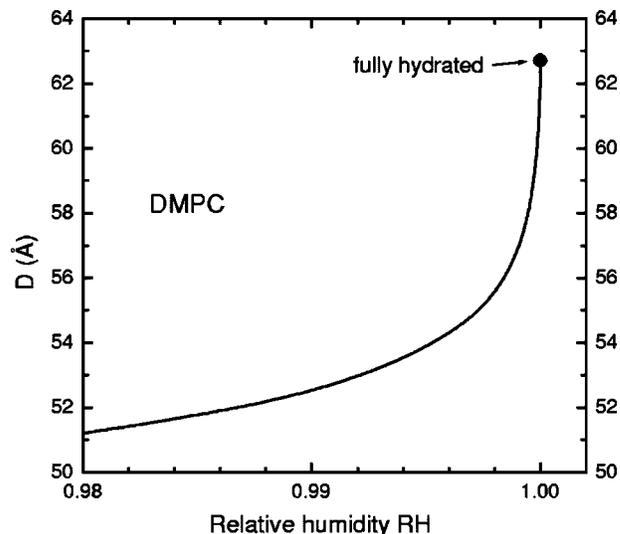
FIG. 3. Relative humidity required to obtain repeat spacing D in DMPC (adapted from [26]).

Achieving full hydration from the vapor is defined as having the same repeat spacing D as for samples (typically unoriented multilamellar vesicles) fully immersed in liquid water. Full hydration of fluid L_α phase lipid samples from water vapor is so difficult that before 1998 it was thought to be impossible and that situation was known as the vapor pressure paradox [11]. However, the vapor pressure paradox was shown to be an artifact [39] and an x-ray chamber was built [40] that sometimes produced full hydration from the vapor [9]. We used a second generation sample chamber that also sometimes produces full hydration, but not always.

We routinely overcome hydration shortfalls by mounting our flat sample on a Peltier element that slightly cools the sample relative to the temperature of the chamber and the water vapor [1]. Because the saturated vapor pressure P_{sat} of water decreases with decreasing temperature, lowering the temperature of the sample while maintaining the same vapor pressure P_v of the warmer water reservoir and chamber effectively raises the relative humidity $\mathcal{R} = P_v / P_{\text{sat}}$ at the sample. Accurate differences of relative humidities from 1 are impossible to measure by conventional humidity meters when $\mathcal{R}$ is close to 1. We obtain the $\mathcal{R}$ by using the lipid itself as an osmometer. Our earlier studies of MLV samples of DMPC [26] followed a now classic method [11] that imposes an osmotic pressure by adding a polymer that competes with the lipid for the water. Our study reported D as a function of osmotic pressure P_{osm} [26], which is related to relative humidity $\mathcal{R}$ by the definition [11]

$$P_{\text{osm}} = -(kT/V_W)\ln(\mathcal{R}), \qquad (2)$$

where $V_W = 30$ Å^3 is the volume of a water molecule. Figure 3 replots the result for DMPC from [26] to emphasize the extreme sensitivity of D to $\mathcal{R}$. For most of the samples in this paper, the D spacing obtained at the synchrotron with no Peltier current was about 58 Å at 30 °C. The information in [26] and Eq. (2) then gives $\mathcal{R} = 0.9995$. Although the use of the Peltier cooler means that the system is not in thermal

equilibrium, the temperature difference between the sample and the chamber required to fully hydrate the sample is only 0.008 °C. The major concern with this procedure is that too much cooling over too long a time floods the sample with a macroscopic layer of liquid water, with the undesirable consequence that the absorption correction for different scattering angles becomes large and hard to determine accurately and the mosaic spread increases due to disruption of the bilayer stacking. This undesirable event was detected by observing strong decreases in intensity of the sharp first and second order peaks and it was avoided by reducing the Peltier current when the D spacing approached the fully hydrated value that had been determined from MLV samples and confirmed from other oriented samples that had been inadvertently flooded.

Although thermal equilibration times were rapid, humidity equilibration for final D took about 90 min. To shorten this time, a large Peltier current was used initially. The D spacing was monitored as a function of time, and smaller Peltier current was used as the target D was approached.

III. THEORY OF ANALYSIS

The theory begins with the discrete version [6,9,41] of the free energy functional in the well-known smectic liquid crystal thermodynamic theory,

$$F_U = \frac{1}{2} \int d\mathbf{r} \sum_{n=0}^{N-1} \{K_C[\nabla_r^2 u_n(\mathbf{r})]^2 + B[u_{n+1}(\mathbf{r}) - u_n(\mathbf{r})]^2\},$$

(3)

which contains two mesoscopic parameters, the bending modulus K_C and the compressibility modulus B. From this harmonic theory the height-height pair correlation functions of the displacement field $u_n(\mathbf{r})$ are obtained and used in the calculation of the scattering structure factor $S(\mathbf{q})$ [3]. $S(\mathbf{q})$ is one of the factors in the ideal scattering intensity $I(\mathbf{q})$ $=S(\mathbf{q})|F(q_z)|^2/q_z$. The other factors are the square of the bilayer form factor $|F(q_z)|^2$ and the Lorentz factor q_z^{-1} for oriented samples. The form factor leads to the electron density profile, as shown recently for a different lipid (DOPC) [10]; a similar analysis for DMPC will be reported in a subsequent paper [42]. The strategy of our analysis [9,10] is to find the material moduli K_C and B by obtaining the best fit of $S(q_x)$ to $I(q_x)$, recognizing that the other factors do not depend on q_x and can therefore be replaced by a constant for each value of q_z.

Our calculation of the theoretical $S_{th}(\mathbf{q})$ from the smectic liquid crystal theory is similar to our previous presentations [9,10,37]. As emphasized there, the $I(\mathbf{q})$ data in images such as Fig. 2 are affected by many experimental considerations that should be accounted for quantitatively, and this is accomplished by modifying the ideal theoretical $S_{th}(\mathbf{q})$ before comparing to the data. These considerations follow. The intensity at a given CCD pixel comes from (a) different parts of q space due to rotation of the sample during data collection and also due to the energy spread of the x rays and (b) different parts of the nonzero sample size (geometric broad-

ening) and different mosaic angles. Furthermore, the finite coherence lengths of the x rays and the finite correlation lengths of the sample impose effective cutoffs L_x, L_y, and L_z in the correlation functions that should be used in the $S(\mathbf{q})$ calculation. The computationally challenging problem of convolving all these with the ideal $S_{th}(\mathbf{q})$ in an efficient program is described in detail elsewhere [37]. When fitting data, many iterations of the $S(\mathbf{q})$ calculation must be performed to obtain the best fit values for K_C and B. This takes on the order of 20 min on current PC computers running at 2 GHz.

For the most studied sample we used the measured mosaic spread of 0.12°, the measured energy dispersion 1.2%, and the known sample size. For the cutoff L_x we used 5000 Å, which is essentially the out-of-scattering-plane x-ray coherence length, and we also used this for L_y, which is an insensitive parameter. The program also allows fitting of these parameters as well as of K_C and B, or any combination thereof. Fitting indicated that the effective L_z was comparable to the perpendicular coherence length and a value of 600 Å was used. After considerable exploration of all the parameters, the data for each sample reported in this paper were uniformly analyzed for K_C and B using the same values of the other parameters for all temperatures. Insignificantly different values of these parameters were used for different samples in earlier CHESS runs.

IV. COMPARISON OF DATA AND FITS

Some of the data in Fig. 2 are shown quantitatively as a function of q_x in Fig. 4. $I(q_x)$ decays more rapidly when q_z $=2\pi h/D \approx 0.1h$ Å^{-1} is near a lamellar order (integer values of h) than when q_z is between orders. As was previously emphasized [9,10], this feature is central to being able to obtain both K_C and B independently.

The model $S(\mathbf{q})$ were fitted to those data with q values within the white boxes in Fig. 2. Data close to specular, $0 < q_x < 0.01$ Å^{-1}, were contaminated by specular reflectivity from the Si substrate and they were not used. The fitting box extended from $q_x=0.01$ to 0.3 Å^{-1}, well into the q_x range where the intensities were constant, so that the fit of the residual background intensity was well determined for each value of q_z. In addition to the global parameters K_C and B, for each value of q_z the fit required a free parameter to account for the overall scaling factor $|F(q_z)|^2/q_z$ and an offset parameter $c(q_z)$ was utilized to accommodate residual background. The primary fit to determine K_C and B did not use data for smaller q_z values because the diffuse scattering was contaminated with mosaic spread from the very strong $h=1$ and 2 peaks and because diffuse scatter was relatively weaker compared to reflectivity than it was in the larger q_z regions in the white boxes in Fig. 2. Because of low signal to noise ratio we did not use data in the primary fit where there was little diffuse scattering due to small values of the form factor $F(q_z)$ such as the $q_z=0.45$ Å^{-1} curve in Fig. 4.

As shown in Fig. 4 the fits to most of the data with q_z values within the white boxes in Fig. 2 are good, although not as good as our earlier results for DOPC [10]. We then fixed these best fit values of K_C and B to fit the data over a wider q_z range using only the linear scaling factors
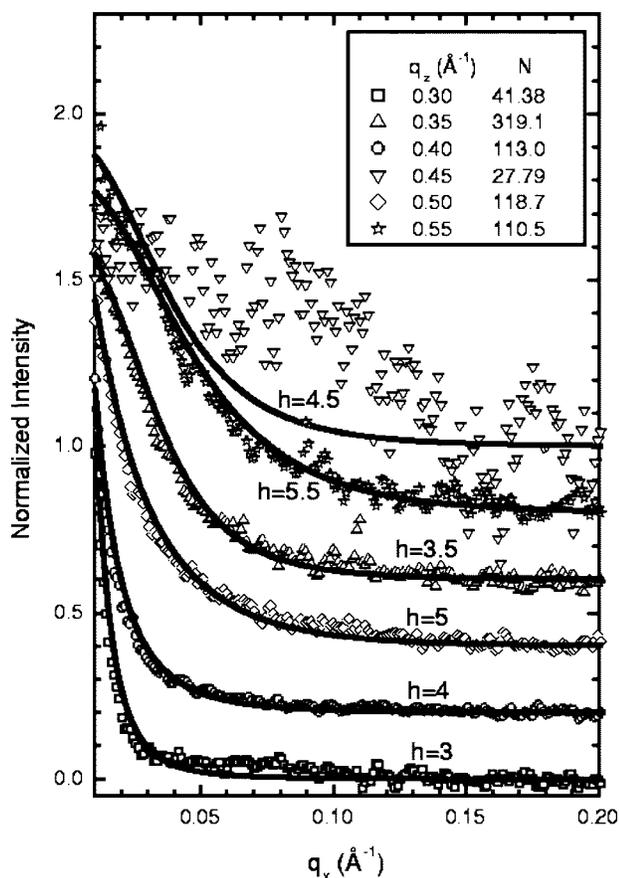
FIG. 4. Normalized scattering intensities I versus q_x for a sample with $D=62.9$ Å at $T=27$ °C are shown as data points for a few values of $h=q_zD/2\pi$ with vertical offsets of 0.2 for successive curves. The solid lines show the fits to the data using the best K_C and B values. The normalization divisors are indicated by the values of N in the legend.

$|F(q_z)|^2/q_z$ and the residual background $c(q_z)$ as free parameters. This extended fit is poor in the region between the two white boxes in Fig. 2, as seen for the $q_z=0.45$ Å^{-1} curve in Fig. 4. This is the region between lobe 2 and lobe 3 where the form factor is essentially zero and the scattering intensities are weak. Instead of decreasing monotonically with increasing q_x these data show a low broad plateau extending to $q_x=0.08$ Å^{-1}. A similar misfit occurs between lobe 1 and lobe 2. That misfit spills over to the $h=3$ curve in Fig. 4 for which q_z is close to the bottom of the lower white box. Because the intensity near the peak is so strong, there is only a relatively small misfit in the 0.05–0.10 Å^{-1} region for $h=3$. These misfits have occurred in many DMPC data sets taken in several different CHESS runs under different experimental conditions. Similar misfits do not occur for DOPC at $T=30$ °C under a similar variety of experimental conditions. Therefore, this appears to be a real phenomenon for DMPC that cannot be accounted for by the smectic liquid crystal theory and may indicate an additional feature, such as coupling of peristaltic fluctuations [43] to undulational fluctuations, that is not present in the smectic theory model. However, a theory for such coupling does not exist, and it is a rather small discrepancy when one compares the small mag-
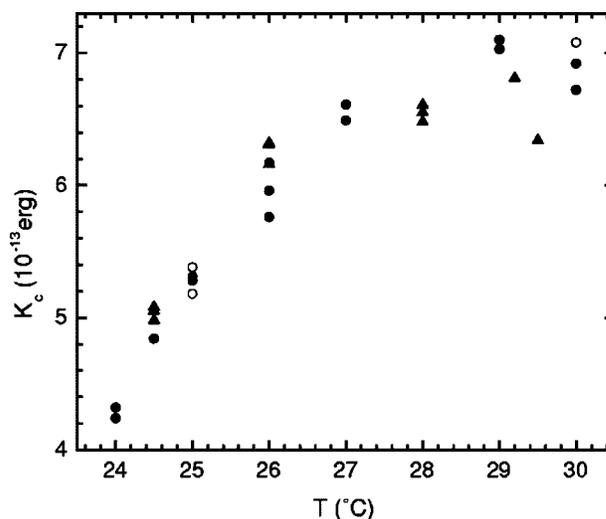
FIG. 5. K_C versus temperature. Different symbols are explained in the text.

nitudes of the misfit intensities with the much larger magnitudes of the well fitted intensities (note the normalization factors in the legend to Fig. 4). We have therefore reported results for K_C using the conventional smectic theory.

V. RESULTS FOR K_C

The temperature dependence of K_C is shown in Fig. 5. Data were also obtained at higher temperatures; $K_C=6.9 \times 10^{-13}$ erg is the same at $T=35$ as at 30 °C and it decreases to about 6.3×10^{-13} erg at 40 °C. A gradual nonanomalous decrease in K_C as T increases above 30 °C is generally expected for the dual reasons that the hydrocarbon core becomes both more fluid and thinner because of the increased disordering of the hydrocarbon chains. This higher temperature behavior is not especially interesting for this paper, so Fig. 5 focuses on the anomalous swelling regime where K_C increases with increasing temperature.

The thermal history of the K_C values shown by solid circles in Fig. 5 is that the sample was first measured at $T=30$ °C. The temperature was subsequently lowered quickly to $T=29$ °C and the sample was thermally equilibrated before measurement. This procedure was repeated for $T=27$, 26, 25, 24.5, and 24 °C. The equilibration time to establish a new D spacing was about 15 min while the time between data collection at successive temperatures typically exceeded 30 min. The different data points at the same temperature were obtained from different CCD exposures. The differences in these values of K_C provide one measure of the experimental uncertainties.

When the temperature was lowered to 23.5 °C, the pattern on the CCD rapidly converted to the distinctive pattern of a ripple phase with clearly distinguishable (h,k) off-meridional peaks (see [44] for typical patterns). Because formation of more ordered, lower temperature phases is often kinetically retarded, this shows that $T=23.5$ °C is a lower bound for the transition T_M. Many measurements of T_M by Nagle and co-workers with precision thermometry and long
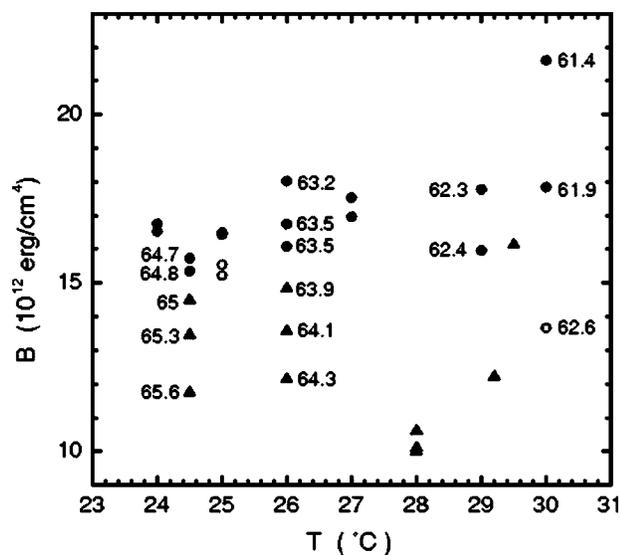
FIG. 6. Compressibility modulus B versus T. Symbols correspond to those in Fig. 5. The numbers beside some of the data points are the repeat spacings D in angstroms.

equilibration times found $T_M = 24.0$ °C [24,45]. Even though ample time was allowed for equilibration, we verified thermodynamical reversibility by raising T first to 25 °C and then back up to 30 °C. These points are shown by open circles in Fig. 5.

We have also taken data on many other samples on other runs at CHESS. The data points shown by solid triangles give results from one of those runs. Comparison with the other data shown give another measure of the experimental uncertainties in K_C. Although none of our previous data had as many data points and the magnitudes of K_C varied somewhat between samples and runs, as indicated by the comparison in Fig. 5, the temperature dependence was generally consistent with the data shown in Fig. 5.

Our value of K_C at $T = 30$ °C in Fig. 5 is only about 25% higher than the value 5.6×10^{-13} erg obtained on giant unilamellar vesicles [29]. In contrast, another method for studying giant unilamellar vesicles reported values of K_C that are roughly twice as large as ours [33]; however, the temperature dependencies of those results, while considerably noisier than ours, are roughly equivalent. It also appears that the inferred decrease in K_C by an order of magnitude in supported double bilayers [16,17] is likely to be an artifact. Our much smaller decrease in K_C is consistent with the alternative, less favored, interpretation [16,17] that formation of a ripple phase in the upper bilayer greatly enhances the swelling that occurs in supported double bilayers below T_M.

VI. RESULTS FOR B

It is of interest to examine the values of the compressibility modulus B that are obtained from the same fits that obtain K_C. Figure 6 shows that the B values differ much more for different data at the same temperature than do the K_C values in Fig. 5. Figure 6 also lists the repeat spacing D (in angstroms) beside many of the data points. Clearly, B decreases
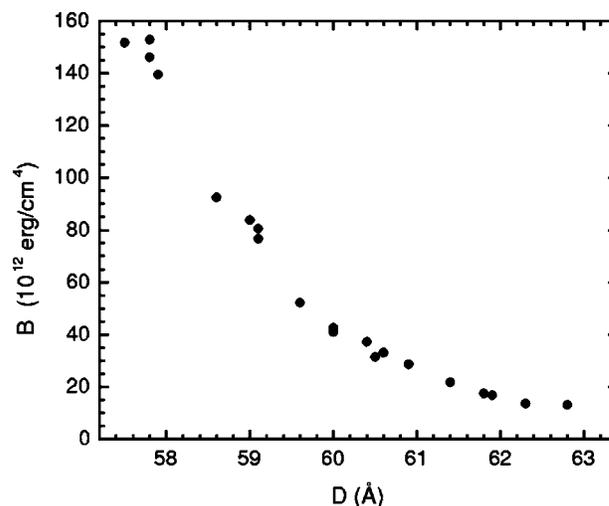
FIG. 7. Compressibility modulus B versus D for $T = 30$ °C.

as D increases for any fixed temperature. This is further illustrated in Fig. 7 for $T = 30$ °C. This behavior is expected because B is a harmonic surrogate for the nonharmonic interactions between adjacent bilayers, and the interactions become weaker as the water spacing increases. Analysis of the interaction strengths responsible for the quantitative behavior in Fig. 7 will be deferred to a subsequent paper. In contrast to the strong variation of B as a function of D, K_C is essentially constant at each T, as indicated in Fig. 5, and as has been shown for the lipid DOPC [10]. This is expected because K_C is the bending modulus for a single bilayer and should not depend upon the interactions between bilayers, at least for uncharged lipid bilayers.

The repeat spacing D varies in our nominally fully hydrated samples because of the difficulty of hydrating lipid bilayers from water vapor. A small decrease of relative humidity from 1 to 0.9999 results in a decrease in D of 2 Å. This can be brought about by a temperature difference of only 0.002 °C between the sample mounted on the sample holder in the middle of the sample chamber and the coolest location on the chamber walls that are regulated by fluid flow from a thermostated water bath. We typically adjusted the Peltier current (see experimental section) to come close to but not above full hydration to avoid flooding the sample. Uncertainties in how much current to use to obtain full hydration and thermal and humidity fluctuations generated a range of D spacings even in our best equilibrated samples. Because of this, it is difficult to obtain $B(T)$ at full hydration without repeating the measurements in Fig. 7 for all temperatures. Despite this uncertainty, the data in Fig. 6 are consistent with a relatively constant value of B in this temperature range. Our data are not inconsistent with the 15% decrease in B previously reported [15], although those data also had large uncertainties. Our data do not support the reported increase in B by a factor of 2 [32]. Intuitively, one might suppose that B should decrease as T approaches T_M because the van der Waals and the hydration interactions decrease with increasing water spacing. However, it has been emphasized [26] that B is not equivalant to these bare interactions, but also includes effects of the fluctuation interaction which is modified by the decrease in K_C.

VII. SIMULATIONS

The temperature dependence of K_C in Fig. 5 is qualitatively similar to the remaining anomalous swelling in Fig. 1. In this section we address whether our measured K_C can quantitatively account for the anomalous swelling by calculating the increase in water spacing. We performed this calculation using a Fourier Monte Carlo mesoscopic simulation specifically devised to treat stacks of bilayers [46]. The simulation was performed on a stack of $M=8$ two-dimensional bilayers, each with linear dimension $L=700$ Å, with periodic boundary conditions in all directions. Each bilayer consisted of $N \times N$ point nodes and the sum of the van der Waals and hydration force interactions were calculated between neighboring nodes on adjacent bilayers. As documented previously [46], results do not vary significantly for larger values of M and L, but an extrapolation with N, using values of N up to 32, is required to obtain accurate results in the lateral continuum limit. The simulation is performed in a constant osmotic pressure ensemble and the output results are the average steric water spacing D'_W and its mean square fluctuations $\sigma^2 = \langle (D'_W - \overline{D'_W})^2 \rangle$.

The purpose of the first set of simulations was to find the value of the Hamaker parameter H that obtains the same repeat spacing D_W as the measured value $D=62.7$ Å at full hydration $(P_{osm}=0)$. We used our measured $K_C=6.9 \times 10^{-13}$ erg at $T=30$ °C, zero osmotic pressure $P_{osm}=0$, and the hydration force parameters from [26] $(P_h=1.32 \times 10^9$ erg/cm^3 and decay length 1.91 Å) and the simulation gave a value of the water spacing D'_W for each trial value of H. To obtain D we added the steric bilayer thickness D'_B which has been given as 44.2 Å at $T=30$ °C [47]; this now changes to 43.4 Å in our structural analysis of the present data [42]. The result is that $D=62.7$ Å is obtained when $H=6.1 \times 10^{-14}$ erg.

The second set of simulations used the value of H obtained above and the measured values of K_C at each T to obtain D'_W as a function of T. The Hamaker parameter and the hydration interaction parameters are assumed not to vary with T [21]. Subtraction of the simulated D'_W at $T=30$ °C gives the anomalous part of D. The simulation result is shown in Fig. 8 where it is compared to the experimental anomalous swelling given by the difference in the two lines in Fig. 1. The outstanding agreement implies that softening of K_C and the ensuing increase in the water space fully accounts for the anomalous swelling above T_M in DMPC.

This conclusion strongly disagrees with the conclusions from previous simulations [21] that softening of K_C could not account for the anomalous swelling. To draw those conclusions required calculation of the Caillé η parameter to compare to measured values of η from unoriented MLV samples. Simulations do not give η directly, but do give the mean square fluctuations σ^2 in water spacing, so the formula

$$\eta = (\pi \sigma / D)^2 \qquad (4)$$

was used. Equation (4) follows directly from the harmonic smectic liquid crystal theory [26] and seemed to be on a solid
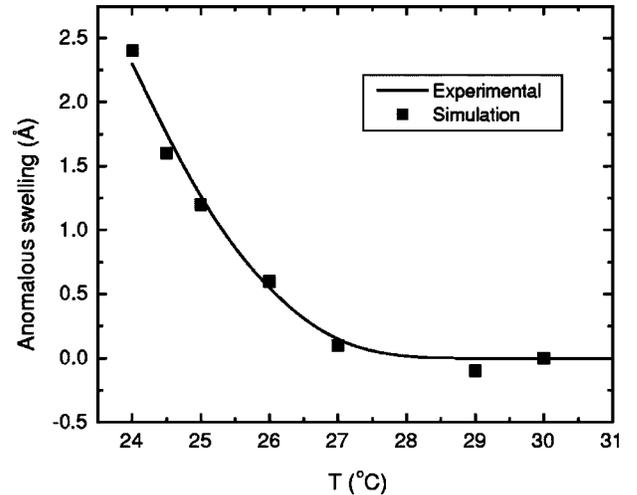
FIG. 8. Comparison of simulated anomalous swelling (solid squares) and measured anomalous swelling (line).

foundation. However, we have begun to be concerned about it because simulations using the detailed form of the interactions cannot obtain both the D spacing and values of σ^2 that agree with our measured values of η. We tentatively attribute this breakdown to the harmonic approximation underlying Eq. (4). We are aware that this explanation also calls into question the use of the harmonic smectic theory to obtain K_C and B. It is, therefore, encouraging that simulations performed using experimental values of K_C work so well to reproduce the observed anomalous swelling in Fig. 8.

The previous simulations also showed that the anomalous swelling that would result from a decrease in K_C would be much smaller when an osmotic pressure $P_{osm}=2.2$ atm was applied than when $P_{osm}=0$ [21]. In contrast, our data [21] and also the more recent data of [15] are in substantial agreement that the anomalous swelling that occurs at $P_{osm}=2.2$ atm is nearly as large as at $P=0$; anomalous swelling is only substantially suppressed at larger $P_{osm}=16$ atm [15]. This disagreement remains when the previous best values of the interactions [26] are used in the simulation. Full resolution of this discrepancy, as mentioned in the introduction, will provide a stringent test of our understanding and determination of all the interactions. This will involve detailed modeling of the data in Fig. 7 that will be deferred to a later paper.

VIII. DISCUSSION AND CONCLUSIONS

The quantitative agreement of simulations and measurements shown in Fig. 8 strongly suggests that anomalous swelling is due to a decrease of K_C as temperature decreases toward the main transition temperature T_M. One important step toward this understanding was to separate the thickening of the membrane from the total swelling of the repeat spacing D. Another important step was to develop a method to measure K_C directly on the same stacks of bilayers that exhibit the anomalous swelling. A third step was to develop Monte Carlo simulations that verify that the measured K_C quantitatively accounts for the anomalous swelling. The

quantitative agreement obtained in Fig. 8 did not require any temperature dependence of the parameters that describe the hydration or van der Waals interactions. This is consistent with previous attempts that failed to justify such temperature dependence [21]. It now appears that further theory of anomalous swelling in lipid bilayers can concentrate on how the quantitative decrease in K_C is brought about by the freezing out of the conformational degrees of freedom in the hydrocarbon chains, which is the thermodynamic driving force for the main transition [28].

[1] S. Tristram-Nagle, Y. Liu, J. Legleiter, and John F. Nagle, Biophys. J. **83**, 3324 (2002).

[2] K. Hristova and S. H. White, Biophys. J. **74**, 2419 (1998).

[3] A. Caillé, C. R. Seances Acad. Sci., Ser. B **274**, 891 (1972).

[4] J. Als-Nielsen, J. D. Litster, R. J. Birgeneau, M. Kaplan, C. R. Safinya, A. Lindegaard-Andersen, and S. Mathiesen, Phys. Rev. B **22**, 312 (1980).

[5] F. Nallet, R. Laversanne, and D. Roux, J. Phys. II **3**, 487 (1993).

[6] N. Lei, C. R. Safinya, and R. F. Bruinsma, J. Phys. II **5**, 1155 (1995).

[7] J. F. Nagle and S. Tristram-Nagle, Biochim. Biophys. Acta **1469**, 159 (2000).

[8] G. Pabst, M. Rappolt, H. Amenitsch, and P. Laggner, Phys. Rev. E **62**, 4000 (2000).

[9] Y. Lyatskaya, Y. Liu, S. Tristram-Nagle, J. Katsaras, and J. F. Nagle, Phys. Rev. E **63**, 011907 (2001).

[10] Y. Liu and J. F. Nagle, Phys. Rev. E **69**, 040901(R) (2004).

[11] R. P. Rand and V. A. Parsegian, Biochim. Biophys. Acta **988**, 351 (1989).

[12] T. J. McIntosh, Curr. Opin. Struct. Biol. **10**, 481 (2000).

[13] T. A. Harroun, M.-P. Nieh, M. J. Watson, V. A. Raghunathan, G. Pabst, M. R. Morrow, and J. Katsaras, Phys. Rev. E **69**, 031906 (2004).

[14] G. Pabst, H. Amenitsch, D. P. Kharakoz, P. Laggner, and M. Rappolt, Phys. Rev. E **70**, 021908 (2004).

[15] G. Pabst, J. Katsaras, V. A. Raghunathan, and M. Rappolt, Langmuir **19**, 1716 (2003).

[16] G. Fragneto, T. Charitat, E. Bellet-Amalric, R. Cubitt, and F. Graner, Langmuir **19**, 7695 (2003).

[17] K. R. Mecke, T. Charitat, and F. Graner, Langmuir **19**, 2080 (2003).

[18] P. C. Mason, J. F. Nagle, R. M. Epand, and J. Katsaras, Phys. Rev. E **63**, 030902(R) (2001).

[19] S. S. Korreman and D. Posselt, Eur. Biophys. J. **30**, 121 (2001).

[20] F. Richter, L. Finegold, and G. Rapp, Phys. Rev. E **59**, 3483 (1999).

[21] J. F. Nagle, H. I. Petrache, N. Gouliaev, S. Tristram-Nagle, Y. Liu, R. M. Suter, and K. Gawrisch, Phys. Rev. E **58**, 7769 (1998).

[22] F. Y. Chen, W. C. Hung, and H. W. Huang, Phys. Rev. Lett. **79**, 4026 (1997).

[23] J. Lemmich, K. Mortensen, J. H. Ipsen, T. Honger, R. Bauer, and O. G. Mouritsen, Phys. Rev. E **53**, 5169 (1996).

[24] R. Zhang, W. Sun, S. Tristram-Nagle, R. L. Headrick, R. M. Suter, and J. F. Nagle, Phys. Rev. Lett. **74**, 2832 (1995).

[25] T. Honger, K. Mortensen, J. H. Ipsen, J. Lemmich, R. Bauer, and O. G. Mouritsen, Phys. Rev. Lett. **72**, 3911 (1994).

[26] H. I. Petrache, N. Gouliaev, S. Tristram-Nagle, R. Zhang, R. M. Suter, and J. F. Nagle, Phys. Rev. E **57**, 7014 (1998).

[27] W. Helfrich, Z. Naturforsch. A **33**, 305 (1978).

[28] J. F. Nagle, Annu. Rev. Phys. Chem. **31**, 157 (1980).

[29] W. Rawicz, K. C. Olbrich, T. McIntosh, D. Needham, and E. Evans, Biophys. J. **79**, 328 (2000).

[30] M. R. Morrow, J. P. Whitehead, and D. Lu, Biophys. J. **63**, 18 (1992).

[31] S. Kirchner and G. Cevc, Europhys. Lett. **23**, 229 (1993).

[32] T. Salditt, M. Vogel, and W. Fenzl, Phys. Rev. Lett. **90**, 178101 (2003).

[33] P. Meleard, C. Gerbeaud, T. Pott, L. Fernandez-Puente, I. Bivas, M. D. Mitov, J. Dufourcq, and P. Bothorel, Biophys. J. **72**, 2616 (1997).

[34] C-H. Lee, W-C. Lin, and J. Wang, Phys. Rev. E **64**, 020901(R) (2003).

[35] S. Tristram-Nagle, R. Zhang, R. M. Suter, C. R. Worthington, W.-J. Sun, and J. F. Nagle, Biophys. J. **64**, 1097 (1993).

[36] J. Als-Nielsen and D. McMorrow, *Elements of Modern X-Ray Physics* (John Wiley & Sons, New York, 2000).

[37] Computational and methodological details about many aspects of this work may be found in Yufeng Liu, Ph. D. thesis, Carnegie Mellon University, 2003, available at http://lipid.phys.cmu.edu

[38] S. L. Barna, M. W. Tate, S. M. Gruner, and E. F. Eikenberry, Rev. Sci. Instrum. **70**, 2927 (1999).

[39] J. Katsaras, Biophys. J. **75**, 2157 (1998).

[40] J. Katsaras and M. J. Watson, Rev. Sci. Instrum. **71**, 1737 (2000).

[41] R. Holyst, Phys. Rev. A **44**, 3692 (1991).

[42] N. Kučerka, Y. Liu, N. Chu, H. I. Petrache, S. Tristram-Nagle, and J. F. Nagle (unpublished).

[43] E. Lindahl and O. Edholm, Biophys. J. **79**, 426 (2000).

[44] J. Katsaras, S. Tristram-Nagle, Y. Liu, R. L. Headrick, E. Fontes, P. C. Mason, and J. F. Nagle, Phys. Rev. E **61**, 5668 (2000).

[45] J. F. Nagle and D. A. Wilkinson, Biophys. J. **23**, 159 (1978).

[46] N. Gouliaev and J. F. Nagle, Phys. Rev. Lett. **81**, 2610 (1998).

[47] H. I. Petrache, S. Tristram-Nagle, and J. F. Nagle, Chem. Phys. Lipids **95**, 83 (1998).